2021 43rd Annual International Conference of the
IEEE Engineering in Medicine & Biology Society (EMBC)
Oct 31 - Nov 4, 2021. Virtual Conference

HingePlace: Focused transcranial electrical current stimulation that allows subthreshold fields outside the stimulation target

Chaitanya Goswami, *Student Member, IEEE* and Pulkit Grover, *Senior Member, IEEE*

***Abstract*— Transcranial Electrical Stimulation (TES) is a promising tool for treating many neurological disorders, but it classically results in diffused stimulation. Many optimization algorithms have been proposed for focusing TES, commonly by creating multi-electrode arrangements and choosing current amplitudes such that the resulting current fields in the brain are focused in the target region, and are as small as possible outside the target region. Consequently, it is likely that such optimization does not harness the non-linear nature of neural dynamics, particularly their thresholding phenomenon, i.e., the observation that neurons fire only when the stimulating currents are above a certain threshold. In this work, we propose *HingePlace* which explicitly harnesses this thresholding phenomenon by designing multi-electrode arrangements which allow the electric fields outside the target region to be non-zero but still below the stimulation threshold. In idealized simulated models, we compare *HingePlace* with existing algorithms and find that *HingePlace* performs strictly better, in some cases providing $\sim$20% reduction in stimulated area for a specified limit on maximum injected current.**

I. INTRODUCTION

Transcranial Electrical Stimulation (TES) is an umbrella term used for either stimulating or modulating the neural activity of the brain using electrical currents delivered from electrodes placed at the scalp. TES is a promising therapeutic tool for many neurological diseases and disorders, including but not limited to clinical depression [1], chronic pain [2], Parkinson's [3], and many more [4].

Traditionally, TES is performed using two large electrodes (a cathode and an anode). This arrangement of electrodes creates a diffused field in the brain causing a widespread stimulation/modulation, even when only a focal stimulation is desired. In recent years, advances have been made (e.g. [5]–[9] and the references therein) on designing multi-electrode TES arrangements and current patterns that create fields which only have significant amplitude in a region of interest (e.g. motor or somatosensory cortex). Such multi-electrode arrangements can improve focality, which can improve the clinical efficacy of TES-based therapies and help develop more precise brain-machine interfaces [5]. In this work, we refer to the problem of designing such electrode montages and the injected current amplitudes as the problem of electrode placement.

This material is based upon work supported by the Naval Information Warfare Center (NIWC) Atlantic and the Defense Advanced Research Projects Agency (DARPA) under Contract No. N65236-19-C-8017. Any opinions, findings and conclusions or recommendations expressed in this material are those of the authors and do not necessarily reflect the views of the NIWC Atlantic and DARPA. CG is also supported by the Centre for Machine Learning and Health (CMLH) fellowship at Carnegie Mellon University. Both authors are with Dept. of Electrical and Computer Engineering, Carnegie Mellon University, 5000 Forbes Avenue, Pittsburgh, USA

Fundamentally, there are two challenges that make the problem of electrode placement hard: a) Laws of physics dictate that the currents generated by the electrodes at the scalp diffuse as they travel through the layers of head, i.e. scalp, skull and cerebrospinal fluid (CSF), making it hard to constrain the area of stimulation; b) the amount of current at each electrode, and the total current that is injected into the scalp, cannot be too high (to avoid pain or tissue damage in the scalp), making it hard to create high-amplitude electric fields in the brain. Existing works formulate the problem of electrode placement as a search/optimization problem [5]–[9]. They divide the brain into two regions: region of interest where we want the field to be high (which we call the *focus* region), and the remaining region of "non-interest" where we want the field to be low (which we call the *cancel* region). The optimization problem is set up in such a way that its solution is an electrode montage that produces the smallest electric field (i.e. as close to zero as possible) in the cancel region, given a desired amplitude of electric field in the focus region (see Sec. III). These algorithms succeed in producing focused fields, and, consequently, focused stimulation, in simplified models (ranging from spherical head models to real-head models), as well as in experiments (as recently tested in [10]).

While the existing electrode placement algorithms [5]–[8] are successful in creating focused electric fields, they do not explicitly take advantage of the non-linear nature of neurons, especially the thresholding phenomenon of neurons [11] (i.e., neurons only fire when the stimulating field is above a certain threshold). For focused *stimulation*, one does not require electric fields to be *minimized* in the cancel region. Instead, it is sufficient that it be below the stimulation threshold (which depends on the stimulating waveform[1], but is fixed for a given waveform). In this work, we propose *HingePlace*, an algorithm for electrode placement that poses an optimization problem that directly exploits the thresholding phenomenon of neurons. *HingePlace* employs a loss function which only becomes non-zero when the electric field is above a user-specified threshold (E_{tol}) in the cancel region, thereby allowing for fields which can have significant non-zero current in the cancel region, but provide more focused neural activation.

In order to quantify the gains of *HingePlace* with respect

[1]For simplicity, we assume that only one neuron-type is present, a simplifying assumption that has been made in prior computational as well (e.g. [9]). This best approximates gyri in the cortex where cortical columns have a fairly regular structure with similar cell-types. However, it is only an approximation, and hence experimental implementations might need to test and adapt accordingly.

to existing algorithms, we compare *HingePlace* with the Directionally Constrained Maximization (DCM) algorithm proposed in [7], in simulated (spherical head) models [12] in Sec. V. DCM was shown in [7] to subsume most of the existing TES electrode placement algorithms proposed in literature, and therefore is a good candidate for comparison. We observe that our method performs strictly better than DCM in terms of the area of stimulation (approximated by area of the electric field above a certain pre-defined threshold), providing as much as $\sim$20% reduction in stimulated area when the allowed injected current at each electrode is moderately high (see Fig. 2).

The paper is structured as follows: Sec. II provides the idealized system model which helps us specify the algorithm. Sec. III makes explicit why existing algorithms minimize the fields outside the region of focus (and not just keep them below a threshold). Sec. IV specifies our optimization framework, *HingePlace*, that aims to only keep the fields outside the focus region below a specified threshold (E_{tol}, the "tolerable" level of the field). Sec. V provides an understanding, using idealized simulations, of when HingePlace can outperform existing techniques in focused stimulation. We conclude in Sec. VI with a discussion, including some limitations of our work.

II. System Model

We assume that, apriori $N \in \mathbb{N}$ locations are chosen on the scalp, where we are allowed to place the electrodes. Let $I = \left[i_1, \ldots, i_N\right]^T \in \mathbb{R}^N$ be an N-dimensional vector, where i_j represents the current injected at the j-th location. If no electrode is placed at the j-th electrode location, then the corresponding $i_j = 0$. Therefore the vector I completely describes an electrode montage, and the problem of electrode placement can be reduced to finding the "optimal" I. A frequent assumption made in electrode placement algorithms is that the physics of the electrode placement problem is governed by the quasi-static Maxwell equations [13]. Therefore, given the conductivities and geometries of all the layers of the head, namely the scalp, the skull, the CSF and the white and grey matter of the brain, and the current (injected by the electrodes) at each of the location, we can calculate the field in the brain using the Laplace equation [13]. The solution of the Laplace equation can be found by discretizing the head model and solving it using a numerical technique such as Finite Element Method (FEM). This discretization yields the following linear system [5], [7]:

$$TI = E_I,\ T \in \mathbb{R}^{3M \times N},\ E_I, \in \mathbb{R}^{3M} \tag{1}$$

where M (typically $\gg$ N) is the number of voxels into which the head model is discretized, E_I is the electric field induced in the head in x, y and z direction (hence the size $3M$), T is the transfer matrix/function that maps the injected currents to the induced electric field E_I. T only depends on the conductivity and geometry of the head model. A more detailed explanation for deriving (1) is provided in [5], [7].

Using the above formulation, the problem of electrode placement can be conceptualized as two sub-problems: a) Defining some desired properties of the electric field E, which we want to induce in the brain (e.g. electric field should be high in the focus region and low in the cancel region) and b) Inverting the over-constrained linear system described in (1) to find the electrode montage described by I, whose electric field E_I satisfies the desired properties, specified in a), as closely as possible (since (1) describes an over-constrained system, it may not be possible to generate an I, whose E_I satisfies all of the desired properties). Usually, an optimization framework is used for finding the optimal I whose induced electric field E_I satisfies the desired properties specified in a), e.g. [5]–[8].

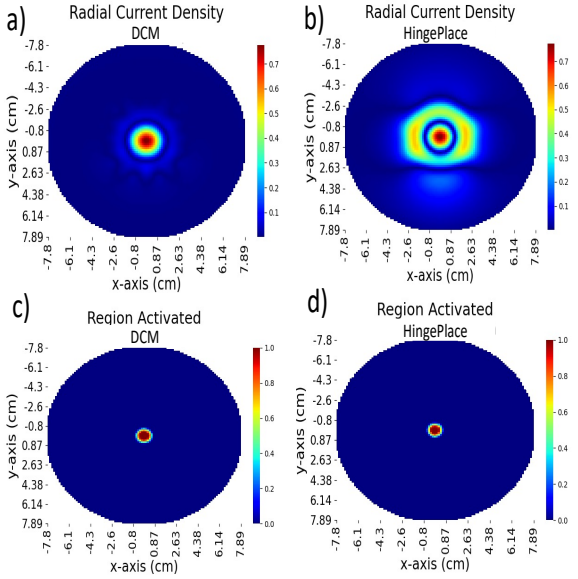

Fig. 1. a) Current Density generated by DCM at the upper hemisphere of the shell at the depth of 1.3 cm projected onto the $x-y$ plane; b) Current Density generated by *HingePlace* at the upper hemisphere of the shell at the depth of 1.3 cm projected onto the $x-y$ plane; c) Corresponding region of the electric field shown in a) that leads to neural stimulation for DCM (approximated by area above 80% of the maximum field (see Sec. V-E)); d) Corresponding region of the electric field shown in a) that leads to neural stimulation for *HingePlace* (approximated by area above 80% of the maximum field (see Sec. V-E)).

III. Limitations of Existing Approaches

In a recent work [7], it was shown that many of the existing algorithms for electrode placement are subsumed by the DCM algorithm. Therefore, by analyzing the DCM algorithm we can gain insight into a wide class of existing algorithms. To that effect, we first give a description of DCM as proposed in [7] in Sec. III-A. While the formulation of DCM presented in III-A does not suggest that DCM minimizes the field in cancel region, an equivalent formulation of DCM is derived in Sec. III-B to show that DCM tries to find the optimal I (see Sec. II) by minimizing the energy of the electric field in the cancel region.

A. Directionally Constrained Maximization

The first step in DCM is to identify a region of interest (focus region) and a region of non-interest (cancel) region.

Let the focus region be denoted by F and the cancel region be denoted by C. Then DCM seeks to maximize the current/electric field intensity along the direction $\vec{d} = [d_x, d_y, d_z]$ in the focus region, while minimizing the field magnitude in the cancel region through the following optimization:

$$\begin{aligned} I^* = \arg\max_I D^T \Gamma_F T_f I, \\ \text{s.t } I^T T_c^T \Gamma_C T_c I \leq \alpha, \quad \|I\|_1 \leq 2I_{tot}, \\ \|I\|_\infty \leq I_{safe}, \quad \mathbf{1}_N^T I = 0. \end{aligned} \tag{2}$$

Let us define and try to understand each term in (2).

The first term $D^T \Gamma_F T_f I$ is a discrete approximation of the integral of the electric field along the direction $\vec{d}$ in the focus region, i.e. $\int_{\vec{r} \in F} \vec{d} \cdot \overrightarrow{E_I}(\vec{r}) dV$. Here, $D \in \mathbb{R}^{3N \times 1}$ is the vector denoting the direction along which the electric field for each voxel in F should be projected. $\Gamma_F \in 3N \times 3|F|$ (where $|F|$ is the number of voxels present in the focus region) is the matrix that results due to the integration operation, and its elements are just volumes of each voxel in the focus region. $T_f \in \mathbb{R}^{3|F| \times N}$ is the matrix constructed from sub-sampling the rows of the transfer matrix T, which correspond to the voxels lying in the focus region F. Therefore $T_f I$ gives us the electric field E_I for each voxel in the focus region. The optimization problem seeks to maximize the integral of electric field along the direction $\vec{d}$ in the focus region, which is equivalent to maximizing the average intensity of the electric field in the focus region along $\vec{d}$.

The quadratic term $I^T T_c^T \Gamma_C T_c I$ represents the energy of the electric field in the cancel region C. The particular form of the quadratic term again stems from discretizing the integral for calculating the energy of the field in the cancel region: $\int_{\vec{r} \in C} \left\| \overrightarrow{E_I}(\vec{r}) \right\|_2^2 dV$. Here, $T_c \in \mathbb{R}^{3|C| \times N}$ (where $|C|$ is the number of voxels present in the cancel region) is the matrix constructed from sub-sampling the rows of the transfer matrix T, which correspond to the voxels lying in the cancel region C, and $\Gamma_C \in 3|C| \times 3|C|$ is the matrix that results due to the integration operation, and is a diagonal matrix with the diagonal elements being just volumes of each voxel in the cancel region. Therefore the constraint $I^T T_c^T \Gamma_C T_c I \leq \alpha$ bounds the electric energy below a certain threshold α.

The constraint $\|I\|_1 \leq 2I_{tot}$ restricts the total current being injected from the electrode montage to I_{tot} and the constraint $\|I\|_\infty \leq I_{safe}$ restricts the maximum current injected per electrode to I_{safe}, to ensure safe stimulation (see Sec. I). The constraint $\mathbf{1}_N^T I = 0$ is present for satisfying the Kirchhoff's law, i.e. the amount of current going into the head should be equal to the amount of current going out ($\mathbf{1}_N$ is just a N-dimensional vector of all ones). For the sake of brevity, throughout this paper we will denote $D^T \Gamma_F T_f$ by A_f, and $I^T T_c^T \Gamma_C T_c I$ by $\|A_c I\|_2^2$ (which also defines A_c).

B. Limitations of DCM

As we mentioned earlier, it is not obvious from the formulation described in (2) that DCM minimizes the electric field in the cancel region. Therefore, in order to prove our claim that DCM minimizes the electric field in the cancel region, we define the following optimization formulation:

$$\begin{aligned} I^* = \arg\min_I \|A_c I\|_2^2, \\ \text{s.t } A_f I = E_{des}, \quad \|I\|_1 \leq 2I_{tot}, \\ \|I\|_\infty \leq I_{safe}, \quad \mathbf{1}_N^T I = 0. \end{aligned} \tag{3}$$

We prove that solving (3) is equivalent to solving (2) (see Appendix). As one can see from (3), the ideal optimal I for DCM would be the one which satisfies $A_c I = 0$, and $A_f I = E_{des}$. Therefore, DCM and by extension all the algorithms subsumed under it over-penalize the electric field in the cancel region and do not try to take advantage of the thresholding phenomenon of neurons.

IV. HingePlace

In this section, we propose *HingePlace*, an optimization framework that explicitly tries to take advantage of the thresholding phenomenon of neurons. The optimization framework is given below:

$$\begin{aligned} I^* = \arg\min_{I \in \mathbb{R}^N} \; & diag(\Gamma_C)^T \max\left(0, T_c I - E_{tol}^+\right) + \\ & diag(\Gamma_C)^T \max\left(0, -T_c I - E_{tol}^-\right), \\ \text{s.t } & A_f I = E_{des}, \quad \|I\|_1 \leq 2I_{tot}, \\ & \|I\|_\infty \leq I_{safe}, \quad \mathbf{1}_N^T I = 0. \end{aligned} \tag{4}$$

where $diag(\Gamma_C) \in \mathbb{R}^{3|C| \times 1}$ is just a vector consisting of all the diagonal elements of Γ_C defined in Sec. III-A, $\max(\cdot)$ is applied element-wise to each of the vector and $E_{tol}^+, E_{tol}^- \in \mathbb{R}^{3|C|}$, whose elements specifies the level of electric field that is tolerable in each voxel of the cancel region. A common choice for E_{tol}^+ and E_{tol}^- is $E_{tol}\mathbf{1}_{3|C|}$, where $\mathbf{1}_{3|C|}$ is the vector of all ones, and E_{tol} is some global level of electric field that is tolerable. For the sake of brevity, we will denote the loss function in (4) as $L_{hinge}(I)$, i.e.

$$\begin{aligned} L_{hinge}(I) = \; & diag(\Gamma_C)^T \max\left(0, T_c I - E_{tol}^+\right) + \\ & diag(\Gamma_C)^T \max\left(0, -T_c I - E_{tol}^-\right). \end{aligned} \tag{5}$$

The only difference between (4) and (3) is in their loss functions, i.e. $L_{hinge}(I)$ for *HingePlace* and an l_2 norm constraint $\|A_c I\|_2^2$ in case of DCM-type approaches. Therefore, in this section we only describe the role of $L_{hinge}(I)$ in *HingePlace*, since the role of constraints in (4) is the same as it was in DCM.

$L_{hinge}(I)$ can be thought of as a discretized version of the following integral: $\int_C \max\left(0, \vec{E}(\vec{r}) - \vec{E}_{tol}^+(\vec{r})\right) + \max\left(0, -\vec{E}(\vec{r}) - \vec{E}_{tol}^-(\vec{r})\right) dV$. On closer inspection, we see that $L_{hinge}(I)$ will have a non-zero value only if any component of $\vec{E}(\vec{r}) \succcurlyeq \vec{E}_{tol}^+(\vec{r})$ or $\vec{E}(\vec{r}) \preccurlyeq -\vec{E}_{tol}^-(\vec{r})$, where $\succcurlyeq, \preccurlyeq$ represent elementwise inequalities. Hence, $L_{hinge}(I)$ only penalizes the electric fields which violate their upper or lower thresholds in the cancel region, thereby allowing fields having non-zero (albeit below pre-defined thresholds) amplitudes in the

cancel region. In contrast, DCM-type approaches try to minimize the electric field and bring them as close to 0 as possible. Because of this, DCM-type approaches are "over-restrictive", i.e. they disallow fields which have significant non-zero electric field (but below the stimulation threshold of neurons) outside the target region (see Fig. 1), even if they provide better focus. In contrast, HingePlace does not penalize such electric fields, and can actually find such fields which can lead to potentially more focused neural stimulation.

V. Results

In this section we perform a comparison between *HingePlace* and DCM by simulating a simplistic head model, and comparing performance across a range of their hyper-parameters ($E_{des}, I_{tot}, I_{safe}$ etc.). For implementing DCM, we use the formulation described in (3), since in that case the hyper-parameters for *HingePlace* and DCM are very similar.

A. Head Model

We use a 4-Sphere Head Model [12], comprising of skull, scalp, CSF, and brain. The conductivities of the scalp, the skull, the CSF and the brain were chosen to be 0.3 S/m, 0.006 S/m, 1.79 S/m and 0.33 S/m., and the thickness of the scalp, the skull and the CSF were chosen to be 6mm, 5mm and 1mm. The conductivity values were taken from [7], and thickness values taken from [12]. The overall head radius was chosen to be 9.2 cm. The forward model for the 4-sphere head model was solved using analytical solutions taken from [14].

B. Electrode Grid

We chose a uniformly spaced electrode grid of 91 electrodes, each having 5 mm diameter, and an inter-electrode spacing of 7mm (measured from one center of one electrode to the center of the other). The electrodes are arranged in a circular patch centered at the north pole. The overall radius of the patch is 4cm.

C. Region of Interest

For the sake of simplicity, we chose the radial current density as preferred direction for stimulation, i.e. the D vector in A_f (see Sec. III-A) points perpendicular to the surface of the cortex. For the focus region, we chose a single point at the north pole at a depth of 1.3cm from the scalp. Since the goal was to compare the focality of the fields produced by the *HingePlace* and DCM, choosing the focus region as a single point provided the most focused fields. The corresponding cancel region was chosen as a hollow ring, with outer radius 3cm and inner radius 0.5cm at the surface of the shell at a depth of 1.3cm from the scalp, with the centre being the focus point. For creating the cancel matrix we sampled this hollow ring uniformly at a spacing of 1mm.

D. Choosing Hyper-parameters

The difficult part of choosing the hyper-parameters E_{des}, I_{safe} and I_{tot} is that they all depend upon each other, and a simple grid search across all of them can be computationally expensive. Furthermore, the value of E_{des} depends upon the kind of waveform being applied, e.g. if we use a DC waveform, then it is believed that the required $E_{des} \approx 0.6V/m$ [15], whereas [16] uses very short pulse stimulation, generating electric field upwards of 50 V/m in the brain. Similarly, the acceptable values of I_{safe} and I_{tot} also depend on the waveform being applied. Therefore to sidestep this problem, we use a conventional 2-electrode configuration (e.g. that used in Transcranial Direct Stimulation or TDCS) to serve as the baseline. With some abuse of nomenclature, we call this "TDCS-type" electrode configurations, as such configurations are commonly used in clinical settings for TDCS, even though here we allow for different (i.e., non-DC) current waveforms to be used. This configuration provides baseline values of E_{des}, I_{tot} and I_{safe} against which other algorithms can be compared.

For simulating TDCS-type electrode configurations, we placed two spherical electrodes of radius 3cm (surface area = 28.3 cm^2), one at the north pole and the other at the south pole of the sphere. The injected current amplitude was chosen such that the current *density* injected by the electrode is 1 mA/cm^2. The figure of 1 mA/cm^2 was chosen arbitrarily, since all the results are reported relative to the parameters for TDCS-type configuration. From the TDCS-type simulation, we calculated the electric field at our focus region (since in our simulation the focus region corresponds to a single point, we just calculated the electric field at that point). The corresponding electric field was $2.6V/m$ at the focus point. This was the E_{des} which we used for both *HingePlace* and DCM. For determining the hyper-parameter I_{safe}, we first calculated I_{init}, which is the current that would inject 1 mA/cm^2 through the electrodes mentioned in Sec. V-B. A simple calculation yields I_{init}= 0.19 mA. Then we ranged across different values of I_{safe} in the following manner I_{safe}[2] $= [10I_{init}, 15I_{init}, 20I_{init}, 25I_{init}, 30I_{init}, 40I_{init}, 45I_{init}, 50I_{init}, 100I_{init}]$. For a given value of I_{safe}, we chose four different values $I_{tot} = [40.5I_{safe}, 20I_{safe}, 12.5I_{safe}, 5I_{safe}]$, corresponding to 4 different situations. $I_{tot} = 40.5I_{safe}$ refers to the situation for which the l_1 constraint in (3) and (4) does not matter, since the maximum current that could be injected due to the l_∞ constraint is $91I_{safe}$, whereas on the other extreme $5I_{safe}$ refers to the condition where l_1 constraint is extremely dominant over the l_∞ constraint in (3) and (4). For *HingePlace*, an additional hyper-parameter needs to be specified, which is E_{tol}. For the tangential direction we chose E_{tol} to be zero and along the radial direction, we chose three values of $E_{tol} = [0.7E_{des}, 0.5E_{des}, 0.1E_{des}]$.

[2]Choosing below $10I_{init}$ results in our constraint set being empty, i.e. there was no possible electrode montage that could generate the required E_{des}

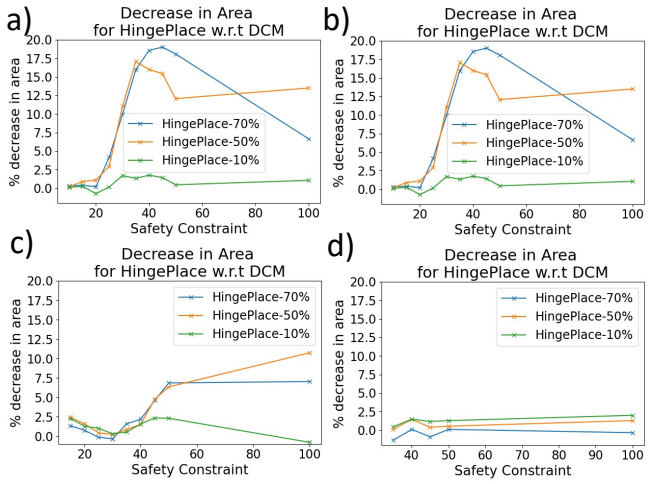

Fig. 2. Plot of the relative decrease in area above 80% for *HingePlace* with respect to DCM for different values of I_{safe}. The x-axis only show the multiplier applied to I_{init} (see Sec. V-D) for different values of I_{tot}: a) $I_{tot} = 40.5I_{safe}$, b) $I_{tot} = 20I_{safe}$, c) $I_{tot} = 12.5I_{safe}$ and d) $I_{tot} = 5I_{safe}$.

E. Simulations

To compare *HingePlace* and DCM, we solved the optimization frameworks for *HingePlace* and DCM, using the CVXPY package [17], [18] in python for the hyper-parameters specified in Sec. V-D. We calculated the corresponding fields induced by both *HingePlace* and DCM at the shell of depth 1.3cm from the surface of the scalp (1mm depth into the brain in our model). Then from this electric field, we approximate the neural response, by calculating the area above 80% of the maximum electric field on that shell. This threshold of 80% is borrowed from a recent paper [19], where authors experimentally calculated the area of the stimulation when exposed to transcranial fields using local field potentials (LFPs) in slices and found that no neural response is observed after the field has decayed to $\sim 80\%$ of its maximum values. However, we expect similar results to hold for other thresholds. The values of resulting area of stimulation are plotted in Fig. 3. We also calculate the relative decrease in area for *HingePlace* with respect to DCM, i.e. $(A_{DCM} - A_h)/A_h$, where A_{DCM} is the area above 80% for DCM approaches and A_h is above 80% for *HingePlace*. The relative decrease is shown in Fig. 2 for different choice of hyper-parameters.

From Fig. 2, we observe that in terms of stimulated area, *HingePlace* always performs at least as well as DCM, with better performance for moderately high I_{safe} and I_{tot}. For $E_{tol} = 0.1E_{des}$, the performance of HingePlace and DCM are almost identical, as expected. One trend we observe is that if either I_{safe} or I_{tot} is too low, both DCM and *HingePlace* perform similarly. This is expected, since for very low I_{safe} or I_{tot}, the constraint set for both DCM and *HingePlace* is very small, therefore their results do not significantly differ. We see that as we increase I_{safe}, the constraint set for both DCM and *HingePlace* starts becoming larger, and we see improvements in the performance of *HingePlace* when compared to DCM, but after a certain point the improvements start decreasing, which is also expected. Since, DCM type approaches are over-restrictive we would expect *HingePlace* to perform much better for moderately sized constraint set, for which the over-restrictiveness of DCM would cause its performance to degrade. For very large constraint sets (the situation where I_{safe} is high), the over-restrictiveness of DCM-type approaches is not a significant issue, and we see the improvements of *HingePlace* decrease.

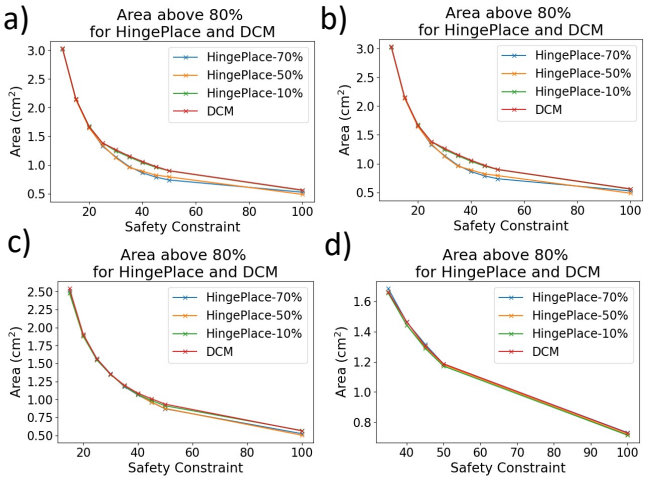

Fig. 3. Plot of the area above 80% for *HingePlace* and DCM for different values of I_{safe}. The x-axis only show the multiplier applied to I_{init} (see Sec. V-D) for different values of I_{tot}: a) $I_{tot} = 40.5I_{safe}$, b) $I_{tot} = 20I_{safe}$, c) $I_{tot} = 12.5I_{safe}$ and d) $I_{tot} = 5I_{safe}$.

VI. Discussion and Conclusion

We described a new approach for electrode placement, *HingePlace*, that explicitly exploits the thresholding phenomenon of neurons to achieve focal neural stimulation. A comparison with DCM, which subsumes a large class of electrode placement algorithms, revealed significant gains in terms of focality for *HingePlace*, *in silico*. The validation in our work is limited to spherical head models here, and comparison of these approaches in more realistic head models remains to be done. We approximate the neural response of the brain to transcranial fields by a simple thresholding function. While it is commonly believed that, to a first order, the neural response can be approximated by a thresholding function (e.g. for fixed waveform shape, and changing amplitude), actual neural responses are quite complex. Hence, an experimental testing of such patterns is needed. There is known to be significant variability in the thresholds of neurons (across types, and even within the same type), which can make choosing the threshold for *HingePlace* difficult, as a high threshold might lead to spurious stimulation in the cancel region, and a low threshold might lose the advantages offered by *HingePlace*. Also, even though electric fields might be low enough for not causing stimulation, they still might modulate the activity of neurons

in *HingePlace*, so care might be needed while using *HingePlace* (e.g. in chronic settings). Despite using the simplest of nonlinear neural response (i.e. thresholding), we still saw significant gains compared to existing algorithms. This shows the potential of incorporating knowledge of neuron-types and neural dynamics while designing TES electrode placement algorithms. Neurons are highly non-linear systems, which makes them hard to analyze but at the same time allows creative strategies to harness this non-linearity to potentially improve performance.

APPENDIX

A general tool for analyzing constrained convex optimization problem is to use Lagrangian duals. First note that l_1 constraint on a N dimensional variable can be represented using 2^N linear inequalities (see Appendix of [7]). We provide an example for representing l_1 constraint for a 3-dimensional vector below:,

$$\|I\|_1 \leq 2I_{tot} \tag{6}$$

$$\Rightarrow \sum_{j=1}^{3} |i_j| \leq 2I_{tot} \tag{7}$$

$$\Rightarrow \begin{bmatrix} 1 & 1 & 1 \\ 1 & 1 & -1 \\ 1 & -1 & 1 \\ 1 & -1 & -1 \\ -1 & 1 & 1 \\ -1 & 1 & -1 \\ -1 & -1 & 1 \\ -1 & -1 & -1 \end{bmatrix} \begin{bmatrix} i_1 \\ i_2 \\ i_3 \end{bmatrix} \preccurlyeq \begin{bmatrix} 2I_{tot} \\ 2I_{tot} \\ 2I_{tot} \end{bmatrix} \tag{8}$$

$$\Rightarrow GI \preccurlyeq 2I_{tot}\mathbf{1}_3 \tag{9}$$

where $\preccurlyeq$ is element wise inequality, and $\mathbf{1}_3$ is the vector of all ones. A similar G can be constructed for the N-dimensional case. Let the i-th row of G be denoted as g_i. Similarly, the l_∞ constraint on a N-dimensional variables can be represented using N inequalities:

$$\|I\|_\infty \leq I_{safe} \tag{10}$$

$$\Rightarrow I_N I \preccurlyeq I_{safe}\mathbf{1}_N, \text{ and } I_N I \succcurlyeq -I_{safe}\mathbf{1}_N \tag{11}$$

where I_N is the identity matrix of size $N \times N$, and $\mathbf{1}_N$ is the N-dimensional vector of all ones. Let the i-th row of I_N be denoted as e_i. Before formulating the K.K.T. conditions, let us write out (2) in the cannonical format:

$$I_1^* = \arg\min_{I_1} -A_f I_1 \tag{12}$$

$$\text{s.t } \|A_c I_1\|_2^2 - \alpha \leq 0, \quad GI_1 - 2I_{tot}\mathbf{1}_{2^N} \preccurlyeq 0$$
$$I_N I_1 - I_{safe}\mathbf{1}_N \preccurlyeq 0 \quad , -I_N I_1 - I_{safe}\mathbf{1}_N \preccurlyeq 0 \tag{13}$$
$$\mathbf{1}_N^T I_1 = 0.$$

Therefore the Lagrangian for DCM can be written as:

$$\mathcal{L}_1 = -A_f I_1 + \lambda^1 \left(\|A_c I_1\|_2^2 - \alpha\right) + \mu^1(\mathbf{1}_N^T I_1) + \sum_{j=1}^{2^N} \delta_j^1(g_j I_1 - 2I_{tot}) + \sum_{j=1}^{N} \nu_j^1(e_j I_1 - I_{safe}) + \sum_{j=1}^{N} \kappa_j^1(-e_j I_1 - I_{safe}) \tag{14}$$

And we can find the optimal solution for the constrained optimization of (2) by using the Lagrangian dual [20]:

$$I_1^*, \lambda^{1*}, \mu^{1*}, \{\delta_j^{1*}\}_{j=1}^{2^N}, \{\nu_j^{1*}, \kappa_j^{1*}\} = \underset{\substack{\lambda^1 \geq 0, \mu^1 \in \mathbb{R}, \\ \{\delta_j^1\}_{j=1}^{2^N} \geq 0, \\ \{\nu_j^1, \kappa_j^1\} \geq 0}}{\arg\max} \; \underset{I_1 \in \mathbb{R}^N}{\arg\min} \mathcal{L}^1 \tag{15}$$

Since, the optimization formulation described in (2) is convex, the solution of the Lagrangian can be found using the K.K.T. conditions [20]. Therefore the solution of (15) should satisfy its K.K.T. conditions (the first is a stationarity condition, and the remaining are complementary-slackness conditions):

$$\left.\frac{\partial \mathcal{L}^1}{\partial I_1}\right|_{I_1 = I_1^*} = -A_f^T + 2\lambda^{1*} A_f^T A_f I_1^* + \mu^{1*}\mathbf{1}_N + \sum_{j=1}^{2^N} \delta_j^{1*} g_j^T + \sum_{j=1}^{N} (\nu_j^{1*} - \kappa_j^{1*}) e_j^T = 0 \tag{16}$$

$$\lambda^{1*}(\|A_c I_1^*\|_2^2 - \alpha) = 0 \tag{17}$$

$$\mathbf{1}_N^T I_1^* = 0 \tag{18}$$

$$\delta^{1*}(g_j I_1^* - 2I_{tot}) = 0 \;\forall\; j \in \{1, \ldots, 2^N\} \tag{19}$$

$$\nu_j^{1*}(e_j I_1^* - I_{safe}) = 0 \;\forall\; j \in \{1, \ldots, N\} \tag{20}$$

$$\kappa_j^{1*}(-e_j I_1^* - I_{safe}) = 0 \;\forall\; j \in \{1, \ldots, N\} \tag{21}$$

Now, in the above system the solution $\lambda^{1*} = 0$ corresponds to $I_1^* = 0$, so it is not useful. So, for the rest of the proof, we will assume that $\lambda^{1*} > 0$. Now, writing the K.K.T. conditions for (3) in exactly the same way as we did for (2). We first write the corresponding Lagrangian for (3):

$$\mathcal{L}^2 = \|A_c I_2\|_2^2 + \beta^2 \left(A_f I_2 - E_{des}\right) + \mu^2(\mathbf{1}_N^T I_2) + \sum_{j=1}^{2^N} \delta_j^2(g_j I_2 - 2I_{tot}) + \sum_{j=1}^{N} \nu_j^2(e_j I_2 - I_{safe}) + \sum_{j=1}^{N} \kappa_j^2(-e_j I_2 - I_{safe}) \tag{22}$$

Again, we can follow the same procedure for optimizing the above Lagrangian to solve for (3)

$$I_2^*, \beta^{2*}, \mu^{2*}, \{\delta_j^{2*}\}_{j=1}^{2^N}, \{\nu_j^{2*}, \kappa_j^{2*}\} = \underset{\substack{\beta^2, \mu^1 \in \mathbb{R}, \\ \{\delta_j^2\}_{j=1}^{2^N} \geq 0, \\ \{\nu_j^2, \kappa_j^2\} \geq 0}}{\arg\max} \; \underset{I_1 \in \mathbb{R}^N}{\arg\min} \mathcal{L}^2 \tag{23}$$

Again, the solution of (23) must satisfy its K.K.T. conditions, which are:

$$\frac{\partial \mathcal{L}^2}{\partial I_2}\bigg|_{I_2=I_2^*} = \beta^{2*}A_f^T + 2A_f^T A_f I_2^* + \mu^{2*}\mathbf{1}_N + \sum_{j=1}^{2^N}\delta_j^{2*}g_j^T +$$

$$\sum_{j=1}^{N}(\nu_j^{2*} - \kappa_j^{2*})e_j^T = 0 \tag{24}$$

$$A_f I_2^* = E_{des} \tag{25}$$

$$\mathbf{1}_N^T I_2^* = 0 \tag{26}$$

$$\delta^{2*}(g_j I_2^* - 2I_{tot}) = 0 \;\forall\; j \in \{1,\dots,2^N\} \tag{27}$$

$$\nu_j^{2*}(e_j I_2^* - I_{safe}) = 0 \;\forall\; j \in \{1,\dots,N\} \tag{28}$$

$$\kappa_j^{2*}(-e_j I_2^* - I_{safe}) = 0 \;\forall\; j \in \{1,\dots,N\} \tag{29}$$

Let us choose $E_{des} = A_f I_1^*$, i.e. the current intensity we found in the DCM optimization (15). Then, we make the following substitution in the equations (24)-(29):

$$I_2^* = I_1^*, \tag{30}$$

$$\beta^{2*} = -\frac{1}{\lambda^*}, \mu^{2*} = \frac{\mu^{1*}}{\lambda^{1*}} \tag{31}$$

$$\delta_j^{2*} = \frac{\delta^{1*}}{\lambda^{1*}} \;\forall\; j \in \{1,\dots,2^N\}, \tag{32}$$

$$\nu_j^{2*} = \frac{\nu^{1*}}{\lambda^{1*}}, \kappa_j^{2*} = \frac{\kappa^{1*}}{\lambda^{1*}} \;\forall\; j \in \{1,\dots,N\} \tag{33}$$

After making the substitutions, we see that

$$\frac{\partial \mathcal{L}^2}{\partial I_2}\bigg|_{I_2=I_1^*} = \frac{1}{\lambda^{1*}}\Bigg(\underbrace{-A_f^T + 2\lambda^{1*}A_f^T A_f I_1^* + \mu^{1*}\mathbf{1}_N}$$

$$+ \underbrace{\sum_{j=1}^{2^N}\delta_j^{1*}g_j^T + \sum_{j=1}^{N}(\nu_j^{1*} - \kappa_j^{1*})e_j^T}_{=0 \text{ due to eq. (16)}}\Bigg) = 0 \tag{34}$$

$$A_f I_1^* = E_{des} = A_f I_1^* \tag{35}$$

$$\underbrace{\mathbf{1}_N^T I_1^*}_{=0 \text{ due to eq. (18)}} = 0 \tag{36}$$

$$\frac{1}{\lambda^{1*}}\left(\underbrace{\delta^{1*}(g_j I_1^* - 2I_{tot})}_{=0 \text{ due to eq. (19)}}\right) = 0 \;\forall\; j \in \{1,\dots,2^N\} \tag{37}$$

$$\frac{1}{\lambda^{1*}}\left(\underbrace{\nu_j^{1*}(e_j I_1^* - I_{safe})}_{=0 \text{ due to eq. (20)}}\right) = 0 \;\forall\; j \in \{1,\dots,N\} \tag{38}$$

$$\frac{1}{\lambda^{1*}}\left(\underbrace{\kappa_j^{1*}(-e_j I_1^* - I_{safe})}_{=0 \text{ due to eq. (21)}}\right) = 0 \;\forall\; j \in \{1,\dots,N\} \tag{39}$$

Therefore the values of $\{I_2^*, \beta^{2*}, \mu^{2*}, \{\delta_j^{2*}\}_{j=1}^{2^N}, \{\nu_j^{2*}, \kappa_j^{2*}\}\}$ given by (30)-(33) satisfy the K.K.T. conditions of (19), thereby are also the solution of (23). Hence, the optimal I we found for both (3) and (2) are the same by the virtue of (30). Therefore we can find solutions of (3) and (2) and vice versa by choosing either $E_{des} = A_f I_1^*$ or $\alpha = \|A_c I_2^*\|_2^2$.

REFERENCES

[1] UG Kalu, CE Sexton, CK Loo, and KP Ebmeier. Transcranial direct current stimulation in the treatment of major depression: a meta-analysis. *Psychological medicine*, 42(9):1791, 2012.

[2] Francesco Mori, Claudia Codecà, Hajime Kusayanagi, Fabrizia Monteleone, Fabio Buttari, Stefania Fiore, Giorgio Bernardi, Giacomo Koch, and Diego Centonze. Effects of anodal transcranial direct current stimulation on chronic neuropathic pain in patients with multiple sclerosis. *The Journal of Pain*, 11(5):436–442, 2010.

[3] Paulo S Boggio, Roberta Ferrucci, Sergio P Rigonatti, Priscila Covre, Michael Nitsche, Alvaro Pascual-Leone, and Felipe Fregni. Effects of transcranial direct current stimulation on working memory in patients with parkinson's disease. *Journal of the neurological sciences*, 249(1):31–38, 2006.

[4] Andre R Brunoni, Felipe Fregni, Alberto Priori, Roberta Ferrucci, and Paulo Sérgio Boggio. Transcranial direct current stimulation: challenges, opportunities, and impact on psychiatry and neurorehabilitation. *Frontiers in psychiatry*, 4:19, 2013.

[5] Jacek P Dmochowski, Abhishek Datta, Marom Bikson, Yuzhuo Su, and Lucas C Parra. Optimized multi-electrode stimulation increases focality and intensity at target. *Journal of neural engineering*, 8(4):046011, 2011.

[6] Yu Huang and Lucas C Parra. Can transcranial electric stimulation with multiple electrodes reach deep targets? *Brain stimulation*, 12(1):30–40, 2019.

[7] Mariano Fernandez-Corazza, Sergei Turovets, and Carlos Horacio Muravchik. Unification of optimal targeting methods in transcranial electrical stimulation. *Neuroimage*, 209:116403, 2020.

[8] Seyhmus Guler, Moritz Dannhauer, Burak Erem, Rob Macleod, Don Tucker, Sergei Turovets, Phan Luu, Deniz Erdogmus, and Dana H Brooks. Optimization of focality and direction in dense electrode array transcranial direct current stimulation (tdcs). *Journal of neural engineering*, 13(3):036020, 2016.

[9] Jiaming Cao and Pulkit Grover. Stimulus: Noninvasive dynamic patterns of neurostimulation using spatio-temporal interference. *IEEE Transactions on Biomedical Engineering*, 67(3):726–737, 2019.

[10] Yu Huang, Anli A Liu, Belen Lafon, Daniel Friedman, Michael Dayan, Xiuyuan Wang, Marom Bikson, Werner K Doyle, Orrin Devinsky, and Lucas C Parra. Measurements and models of electric fields in the in vivo human brain during transcranial electric stimulation. *elife*, 6:e18834, 2017.

[11] Eric R Kandel, James H Schwartz, Thomas M Jessell, Steven Siegelbaum, A James Hudspeth, and Sarah Mack. *Principles of neural science*, volume 4. McGraw-hill New York, 2000.

[12] Paul L Nunez, Ramesh Srinivasan, et al. *Electric fields of the brain: the neurophysics of EEG*. Oxford University Press, USA, 2006.

[13] David J Griffiths. Introduction to electrodynamics, 2005.

[14] Mats Forssell, Chaitanya Goswami, Ashwati Krishnan, Maysamreza Chamanzar, and Pulkit Grover. Effect of skull thickness and conductivity on current propagation for noninvasively injected currents. *Journal of Neural Engineering*, 2021.

[15] Anli Liu, Mihály Vöröslakos, Greg Kronberg, Simon Henin, Matthew R Krause, Yu Huang, Alexander Opitz, Ashesh Mehta, Christopher C Pack, Bart Krekelberg, et al. Immediate neurophysiological effects of transcranial electrical stimulation. *Nature communications*, 9(1):1–12, 2018.

[16] PA Merton and HB Morton. Stimulation of the cerebral cortex in the intact human subject. *Nature*, 285(5762):227–227, 1980.

[17] Steven Diamond and Stephen Boyd. CVXPY: A Python-embedded modeling language for convex optimization. *Journal of Machine Learning Research*, 17(83):1–5, 2016.

[18] Akshay Agrawal, Robin Verschueren, Steven Diamond, and Stephen Boyd. A rewriting system for convex optimization problems. *Journal of Control and Decision*, 5(1):42–60, 2018.

[19] Mats Forssell, Vishal Jain, Chaitanya Goswami, Sara Caldas-Martinez, Pulkit Grover, and Maysam Chamanzar. Effect of focality of transcranial currents on neural responses. In *2021 10th International IEEE/EMBS Conference on Neural Engineering (NER)*. IEEE, 2021.

[20] Stephen Boyd and Lieven Vandenberghe. *Convex optimization*. Cambridge university press, 2004.